CAR-TR-735
CS-TR-3349

DAAH-0493G0419
September 1994

Estimation of Unstabilized Components in Vehicular Motion

Yi-Sheng Yao
Rama Chellappa*

Department of Electrical Engineering
*Institute for Advanced Computer Studies and
Computer Vision Laboratory
Center for Automation Research
University of Maryland
College Park, MD 20742-3275

CAR-TR-735
CS-TR-3349

DAAH-0493G0419
September 1994

Estimation of Unstabilized Components in Vehicular Motion

Yi-Sheng Yao
Rama Chellappa*

Department of Electrical Engineering
*Institute for Advanced Computer Studies and
Computer Vision Laboratory
Center for Automation Research
University of Maryland
College Park, MD 20742-3275

Abstract

This paper presents a kinetic-model based algorithm for estimating some unstabilized components in vehicular motion. In addition to smooth movement, there are unstabilized components such as bounce, pitch and roll in vehicular motion. To reliably accomplish other tasks like tracking and obstacle avoidance using visual inputs, it is essential to consider these disturbances. A two-wheel vehicle model available in the literature is used for this purpose. It takes into account the bouncing and pitching components. The dynamics of these unstabilized components are formulated using standard equations of motion. Assuming that depth information is known for some landmarks in the scene (e.g., obtained from a laser range finder) and additional information from inertial sensors such as accelerometers is available, a feature-based approach is proposed to estimate the unstabilized components. Simulation results for both deterministic and stochastic terrain profiles are presented. The robustness of the filter with respect to various parameter mismatches is also addressed.

The support of the Advanced Research Projects Agency (ARPA Order No. A422) and the Army Research Office under Grant DAAH-0493G0419 is gratefully acknowledged, as is the help of Sandy German in preparing this paper.

1 Introduction

There has been growing interest among computer vision researchers in solving the problem of autonomous vehicle navigation. For many navigation-related tasks such as feature tracking, moving object detection, obstacle avoidance, etc., knowledge of the vehicle's pose and motion is a prerequisite for success. Although the Inertial Navigation System (INS) on board the vehicle can provide accurate attitude and motion information over short periods, there exist some problems over long periods due to sensor drifts. An independent estimate of the vehicle's motion can be combined with the INS data to provide more reliable information.

In recent years, the wealth of information contained in long sequences of images has attracted the attention of computer vision researchers. Due to lack of knowledge of the forces and torques that result in movements of the camera, most kinematic-model-based motion estimation algorithms assume a smooth trajectory over time in order to exploit temporal information [1, 11–14]. However, for a vehicle moving in an outdoor environment, the onboard camera undergoes non-smooth motion. The performance of algorithms which do not take into account unstabilized components in the motion may degrade, as noted in [4].

In order to describe jerky movements of a vehicle, a two-wheel vehicle model which can be found in the literature on optimal design of suspension systems is utilized [2]. This model accounts for two unstabilized components of the motion: bounce and pitch. In addition to compensation for the smooth motion assumption, the explicit separation of unstabilized and stabilized components provides useful information for stabilizing all the sensors on the vehicle.

In this paper, to estimate these components, the equations of motion are first derived from the Lagrangian point of view. Subsequently, assuming that a camera is rigidly attached to the vehicle with known orientation and the 3-D coordinates of some landmarks are available (these can be obtained, for example, by a vehicle-mounted laser range finder), the relationships between the vehicular motion and image plane displacements of these landmarks are found. A recursive algorithm is then formulated, and an Iterated Extended Kalman Filter (IEKF) [7] is used to estimate both unstabilized components of the vehicular motion. In addition to the visual information, inertial sensors such as accelerometers are also incorporated in our work. Since the model requires various internal parameters such as the moment of inertia and the position of the center of gravity, the robustness of the filter with respect to parameter mismatches is also studied analytically and numerically.

The organization of this paper is as follows. Section 2 gives detailed descriptions of the two-wheel vehicle model and the physical laws describing the dynamics of both unstabilized components. The recursive formulation of the algorithm is given in Section 3. Section 4 presents simulation results. A sensitivity analysis is given in Section 5, and conclusions are presented in Section 6.

2 Vehicle Model

In order to account for unstabilized components such as bounce and pitch in vehicular motion, the two-wheel vehicle model [2] shown in Figure 1 is used. Both front and rear tires are modeled by linear springs with the same stiffness coefficient K_T. M_{wf} and M_{wr} represent the masses of unsprung elements such as the front and rear wheels and their axles. K_f, C_f, K_r and C_r are the characteristics of the linear springs and shock absorbers that model the suspension system. W_A and W_B constitute the wheel base and consequently specify the position of the center of gravity of the sprung element (or vehicle body).

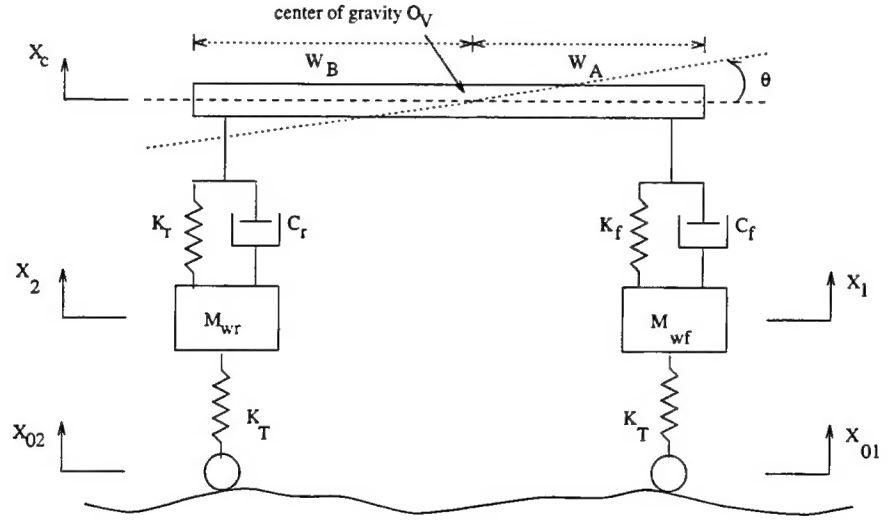

Figure 1: The two-wheel vehicle model [2]

Assuming that each tire contacts the terrain at a point at all times, four degrees of freedom exist in the model: the displacements of the unsprung elements $\{x_1, x_2\}$, the bouncing displacement of the sprung element x_c, and the pitch angle θ. All of them are measured from the corresponding static equilibrium points.

In the following, a coordinate transformation between two moving reference systems is described first. The equations of motion are subsequently derived.

2.1 Coordinate Transformation

To describe the orientation of the vehicle at any time, the coordinate systems shown in Figure 2 are defined. An inertial coordinate system I is chosen to be fixed on the ground. Another coordinate system V moves with the vehicle with its origin locating at the vehicle's center of gravity and its axes coinciding with the principal axes of the vehicle body. For the two-wheel vehicle model, since only the longitudinal axis changes with time, the orientation of the vehicle is known if the pitch angle is available. In other words, if we define the coordinate system I' as the reference system which translates with the vehicle but has the same orientation as reference I, then for any point P, its coordinates in V (denoted by P_V) are related to its coordinates $P_{I'}$ in I' as follows:

$$P_V = RP_{I'} \tag{1}$$

where R is the rotation matrix and is related to the pitch angle by

$$R = \begin{pmatrix} \cos\theta & 0 & -\sin\theta \\ 0 & 1 & 0 \\ \sin\theta & 0 & \cos\theta \end{pmatrix} \tag{2}$$

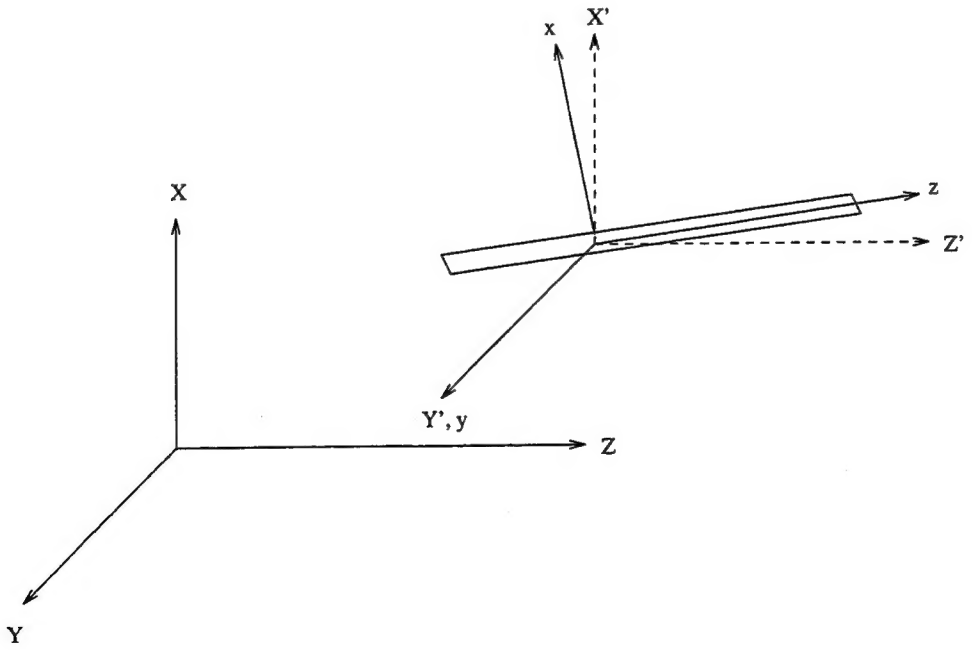

Figure 2: The coordinate systems: The inertial coordinate system I_{XYZ}, the moving coordinate system $I'_{X'Y'Z'}$ and the vehicle coordinate system V_{xyz}.

2.2 Suspension Dynamics

To describe the oscillation behavior of the vehicle model, either the Newtonian laws [9] or Lagrange's equations of motion [3] can be applied. Because of the simplicity of the two-wheel model, it is easy to employ the Newtonian laws. However, for a more complicated model such as a four-wheel vehicle model [5, 10], the Lagrange point of view is more feasible. The equations of motion are therefore derived in terms of Lagrangian mechanics in this paper.

Since there exist four degrees of freedom in the model, define the generalized coordinates as

$$\underline{q} \equiv (x_1, x_2, x_c, \theta) \tag{3}$$

The Lagrange equations of motion can then be written as follows [3]:

$$\frac{d}{dt}\left(\frac{\partial T}{\partial \dot{q}_j}\right) - \frac{\partial T}{\partial q_j} + \frac{\partial U}{\partial q_j} + \frac{\partial D}{\partial \dot{q}_j} = Q_j \quad j = 1, \ldots, 4 \tag{4}$$

where $\{q_j, j = 1, \ldots, 4\}$ constitute the generalized coordinates, T is the kinetic energy of the system, U is the potential energy, D is the dissipation function, and the Q_j's represent the generalized forces acting on the system during vibration. We describe each energy term in the following.

A. Kinetic Energy

It is well known that the kinetic energy of a moving rigid body is equal to the summation of translational kinetic energy and rotational kinetic energy. In other words, if a rigid body moves with translational velocity $\underline{V}$ and angular velocity $\underline{\omega}$, its kinetic energy is [9]

$$\frac{1}{2}M|\underline{V}|^2 + \frac{1}{2}(I_{xx}\omega_x^2 + I_{yy}\omega_y^2 + I_{zz}\omega_z^2) \tag{5}$$

where M is the mass of the rigid body, $\{I_{xx}, I_{yy}, I_{zz}\}$ are the moments of inertia with respect to the principal axes, and $(\omega_x, \omega_y, \omega_z)$ are the projections of the angular velocity along the principal axes.

As seen from Figure 2, since the two-wheel vehicle model only accounts for the bouncing and pitching motion, its rotation axis coincides with the pitch axis at all times. The angular velocity is therefore decomposed into

$$\begin{aligned} \omega_x &= 0 \\ \omega_y &= \dot{\theta} \\ \omega_z &= 0 \end{aligned} \tag{6}$$

Then, taking into account the vertical displacements of the unsprung elements and the oscillation of the sprung element, the kinetic energy can be obtained as

$$T = T_B + T_w \tag{7}$$

where T_B is the kinetic energy contributed from the sprung element

$$T_B = \frac{1}{2} M_B \dot{x}_c^2 + \frac{1}{2} I_{yy} \dot{\theta}^2. \tag{8}$$

Here M_B denotes the mass of the sprung element and T_w is the kinetic energy contributed from unsprung elements

$$T_w = \frac{1}{2} M_{wf} \dot{x}_1^2 + \frac{1}{2} M_{wr} \dot{x}_2^2 \tag{9}$$

B. Potential Energy

The potential energy takes into account the influence of the springs and tires on the vehicle during vibration. Consequently, to obtain the potential energy, the deformations of both elements need to be known. For the tires, the deformations are directly observed from Figure 1 and are obtained as

$$\begin{aligned} d_1 &= x_1 - x_{01} \\ d_3 &= x_2 - x_{02} \end{aligned} \tag{10}$$

On the other hand, noting that the two corners to which springs and shock absorbers are attached remain fixed in the coordinate system V, the deformations of the springs are obtained, by considering the displacement of center of gravity and (1), as

$$\begin{aligned} d_2 &= x_c + W_A \sin\theta - x_1 \\ d_4 &= x_c - W_B \sin\theta - x_2 \end{aligned} \tag{11}$$

Then, assuming linear relationships hold between the deformations and the forces exerted by the springs, the potential energy can be written as

$$U = U_S + U_T \tag{12}$$

where U_S contains the potential energy stored in the suspension systems

$$U_S = \frac{1}{2} K_f d_2^2 + \frac{1}{2} K_r d_4^2 \tag{13}$$

and U_T represents the potential energy stored in the tires

$$U_T = \frac{1}{2} K_T d_1^2 + \frac{1}{2} K_T d_3^2 \tag{14}$$

C. Dissipation Function

The dissipation function accounts for the effect of the shock absorbers. Assuming that the forces produced by dampers vary linearly with the rates of change of the deformations, the dissipation function D is obtained as

$$D = \frac{1}{2}C_f\dot{d}_2^2 + \frac{1}{2}C_r\dot{d}_4^2 \tag{15}$$

In addition to the various forms of energy described above, the generalized force Q_j in (4), which takes into account other factors such as the road reactions on the tires due to tire load variations, is required to describe the jerky movements of the vehicle. The effects of generalized forces will be considered in subsequent sections. Then, by applying (4), the equations of motion can be obtained.

3 Recursive Formulation

It is observed that the resulting equations of motion are nonlinear. For a vehicle traveling through uneven terrain, it is reasonable to expect that the pitch angle is small. Therefore, in deriving the equations of motion, if we further assume that the small pitch angle approximation holds, i.e.

$$\sin\theta \approx \theta \tag{16}$$

then the equations of motion can be described by the following second order, linear differential equation:

$$\ddot{\underline{q}} + K\dot{\underline{q}} + L\underline{q} = M\underline{x}_0 + N\underline{Q} \tag{17}$$

where the elements of the matrices K, L, M and N are related to system parameters such as spring constants, moments of inertia, etc. $\underline{x}_0$ are the excitation inputs and $\underline{Q}$ are the generalized forces defined as

$$\underline{x}_0 = (x_{01}, x_{02}) \tag{18}$$

$$\underline{Q} = (Q_1, Q_2, Q_3, Q_4) \tag{19}$$

If the terrain profile and the generalized forces are known, the bouncing and pitching movements can be obtained through the integration of (17). However, since the system parameters are usually known approximately, the results obtained from direct integration are not reliable. It is therefore feasible to employ some estimation technique and combine the information provided by other sensors such as cameras and accelerometers.

Unlike batch estimators, which process all the data, recursive filters update the estimates of parameters as new information becomes available. Among recursive estimators, EKF and IEKF are both suitable for estimating parameters of a nonlinear system. We describe the plant and measurement equations for the recursive algorithm in the following.

3.1 The Plant Equation

In addition to the imperfect knowledge of system parameters, it is usually difficult to measure the terrain profile and the generalized forces accurately. To account for these difficulties, accelerometers are assumed to be at our disposal to provide the accelerations of unsprung elements. By integration of measured accelerations, the velocities and displacements of unsprung elements are approximately derived.

Therefore, the bouncing displacement and the pitch angle are the remaining unknown quantities. Let the state vector $\underline{x}$ be defined as follows:

$$\underline{x} \equiv (x_c, \dot{x}_c, \theta, \dot{\theta}, v)^T \tag{20}$$

Then under the assumption that the vehicle moves along a straight path with constant forward speed v, the equations of motion can be rewritten in the following form:

$$\dot{\underline{x}} = A\underline{x} + B\underline{x}_w + \underline{w} \tag{21}$$

where $\underline{x}_w$ are regarded as control inputs consisting of displacements and velocities of unsprung elements, i.e.

$$\underline{x}_w = (x_1, \dot{x}_1, x_2, \dot{x}_2)^T \tag{22}$$

A, B are the plant and input matrices derivable from K and L and have the following form:

$$A = \begin{pmatrix} 0 & 1 & 0 & 0 & 0 \\ \frac{-(K_f+K_r)}{M_B} & \frac{-(C_f+C_r)}{M_B} & \frac{-(K_f W_A - K_r W_B)}{M_B} & \frac{-(C_f W_A - C_r W_B)}{M_B} & 0 \\ 0 & 0 & 0 & 1 & 0 \\ \frac{-(K_f W_A - K_r W_B)}{I_{yy}} & \frac{-(C_f W_A - C_r W_B)}{I_{yy}} & \frac{-(K_f W_A^2 + K_r W_B^2)}{I_{yy}} & \frac{-(C_f W_A^2 + C_r W_B^2)}{I_{yy}} & 0 \\ 0 & 0 & 0 & 0 & 0 \end{pmatrix} \tag{23}$$

and

$$B = \begin{pmatrix} 0 & 0 & 0 & 0 \\ \frac{K_f}{M_B} & \frac{C_f}{M_B} & \frac{K_r}{M_B} & \frac{C_r}{M_B} \\ 0 & 0 & 0 & 0 \\ \frac{K_f W_A}{I_{yy}} & \frac{C_f W_A}{I_{yy}} & \frac{-K_r W_B}{I_{yy}} & \frac{-C_r W_B}{I_{yy}} \\ 0 & 0 & 0 & 0 \end{pmatrix} \tag{24}$$

$\underline{w}$ is the plant noise, with zero mean and covariance matrix Q_w. The added plant noise takes into consideration the modeling error and the imprecise knowledge of vehicle parameters as well as the movements of unsprung elements.

3.2 The Measurement Equations

A sequence of images taken by a camera rigidly mounted on the moving vehicle provides visual information for estimating jerky movements. In order to exploit this information, the relationships between the state vector defined above and the image plane coordinates of a set of landmarks need to be derived.

For clarity, in addition to the coordinate systems defined in Section 2.1, define another reference system as a camera coordinate system which has a fixed orientation with respect to the moving reference V and its origin, O_C, located at the projection center of the camera. In other words,

$$O_{CV}(t) = (d_0, 0, l) \quad \forall t \tag{25}$$

where both d_0 and l are constants. Moreover, for a vehicle undergoing bouncing and pitching motion as well as constant longitudinal motion, its center of gravity, O_V, follows the following trajectory expressed in the inertial coordinate system I:

$$O_{VI}(t) = (x_c(t) + h, 0, vt) \quad \forall t \tag{26}$$

where h is the height of center of gravity when the vehicle is at rest.

Then, for a landmark P, the relationships between its inertial coordinates, $P_I = (X_0, Y_0, Z_0)^T$, and the camera centered coordinates, $P_C(t)$, can be found as follows:

$$P_C(t) = R(\theta) \left[\begin{pmatrix} X_0 \\ Y_0 \\ Z_0 \end{pmatrix} - \begin{pmatrix} x_c(t) + h \\ 0 \\ vt \end{pmatrix} \right] - \begin{pmatrix} d_0 \\ 0 \\ l \end{pmatrix} \tag{27}$$

where $R(\theta)$ is the rotation matrix defined in (2). Without loss of generality, it has been assumed that the camera coordinate system has the same pose as the vehicle reference system V.

After the camera centered coordinates have been obtained, the image plane coordinates of landmarks are obtained by applying the perspective projection formula. The resulting measurement equations for the j^{th} landmark are

$$\begin{aligned} X_j(t_i) &= f\frac{\cos\theta(t_i)[X_{0j} - (x_c(t_i)+h)] - \sin\theta(t_i)[Z_{0j} - vt_i] - d_0}{\sin\theta(t_i)[X_{0j} - (x_c(t_i)+h)] + \cos\theta(t_i)[Z_{0j} - vt_i] - l} + n_{X_j}(t_i) \quad j = 1, \ldots, N \\ Y_j(t_i) &= f\frac{Y_{0j}}{\sin\theta(t_i)[X_{0j} - (x_c(t_i)+h)] + \cos\theta(t_i)[Z_{0j} - vt_i] - l} + n_{Y_j}(t_i) \end{aligned} \tag{28}$$

where f is the focal length and N is the number of tracked landmarks. $(n_{X_j}(t_i), n_{Y_j}(t_i))$ is the measurement noise which takes into account the quantization noise and errors in tracking feature points over the sequence.

4 Simulation Results

Using the nominal values of the vehicle parameters listed in Table 1, the performance of the algorithm in estimating the unstabilized components of the vehicle's motion was studied through simulations. Since the movements of unsprung elements due to uneven terrain and generalized forces are approximately known because of the employment of accelerometers, the effects of generalized forces need not be considered separately. The generalized forces are therefore assumed to be zero in the simulations. Then, after the terrain profile is generated, state trajectories obtained through the integration of (17) are regarded as the ground truth for evaluating the filter's performance.

Table 1: Model parameters

M_{wf}	57.5 kg	K_f	18.0 kN $\cdot$ m^{-1}	W_A	1.353 m
M_{wr}	75.0 kg	C_f	1.0 kN $\cdot$ m $\cdot$ s^{-1}	W_B	1.337 m
M_B	1710.0 kg	K_r	10.0 kN $\cdot$ m^{-1}	h	2.0 m
I_{yy}	1031.25 kg $\cdot$ m^2	C_r	1.0 kN $\cdot$ m $\cdot$ s^{-1}	d_0	0.6 m
		K_T	200.0 kN $\cdot$ m^{-1}	l	1.35 m

In the following, the simulation results for different terrain profiles are presented.

4.1 Deterministic Excitation

Consider the behavior of the model when the vehicle encounters a bump. The bump is modeled by a half sine wave with its height and width denoted by b_h and b_w respectively. The movement of the vehicle is such that it first traverses a flat path before encountering the bump, and the front tire hits the bump at the location z_0. After the vehicle passes through the bump, its excitation inputs are zero. This results in an excitation input of the front tire of the following form:

$$x_{01}(t) = \begin{cases} b_h \sin[\frac{\pi}{b_w}(vt - z_0)] & \frac{z_0}{v} \leq t \leq \frac{z_0 + b_w}{v} \\ 0 & \text{elsewhere} \end{cases} \tag{29}$$

In our work, we assumed $b_h = 0.1$ m, $b_w = 0.2$ m and $z_0 = 1.345$ m.

Since the vehicle is assumed to move along a straight path, the rear tire input is related to the front tire input by

$$x_{02}(t) = x_{01}\left(t - \frac{L}{v}\right) \tag{30}$$

where L is the wheel base. Because the excitation inputs to the tires are zero initially, the vehicle is assumed to be in a static equilibrium state with a forward speed of $1.345\ \text{m} \cdot \text{s}^{-1}$. The resulting behavior of the model is displayed in Figure 3.

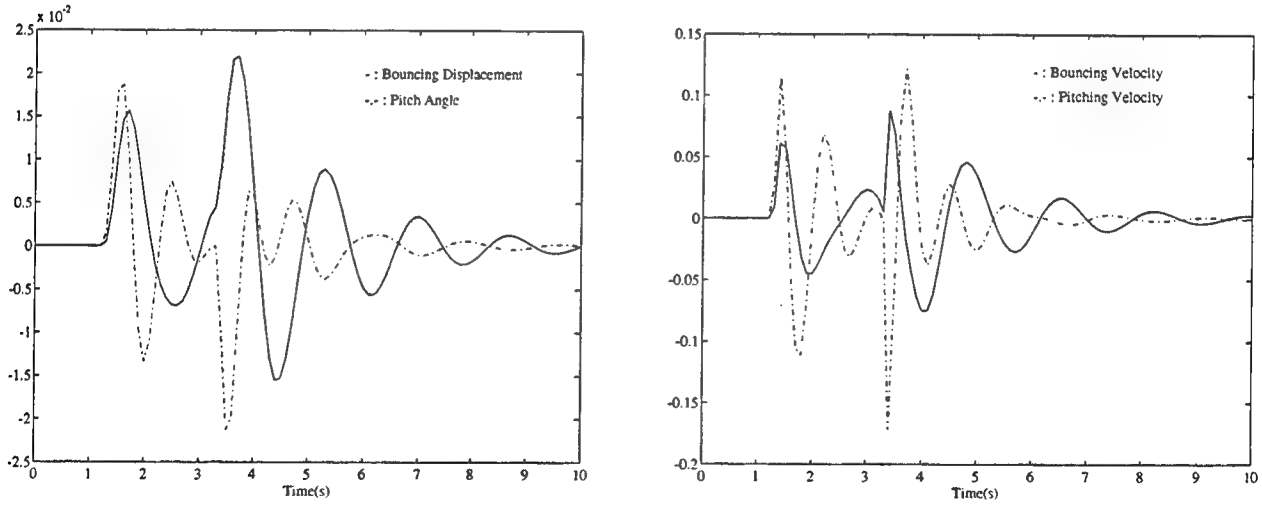

(a) (b)

Figure 3: The movement of the sprung element under the excitation of a bump: (a) The bouncing displacement and the pitch angle; (b) the bouncing velocity and the pitching velocity.

Subsequently, a set of landmarks is tracked over the sequence. Since the image displacement fields due to bouncing and pitching movements are very similar, it is important that the landmarks

being tracked carry enough information for estimation of the unstabilized components. For example, tracking feature points which are far away from the camera provides more information for estimating the pitching motion than the bouncing behavior. This can be seen from (28). By dividing the numerator and denominator by $Z_{0j} - l$, the image plane coordinates for the j^{th} landmark are the same but the measurement equation can be rewritten as

$$X_j(t_i) = f\frac{\cos\theta(t_i)[X_j(t_0) + \frac{d_0}{Z_{0j}-l} - \frac{x_c(t_i)}{Z_{0j}-l}] - \sin\theta(t_i)[1 + \frac{l}{Z_{0j}-l} - \frac{v}{Z_{0j}-l}t_i] - \frac{d_0}{Z_{0j}-l}}{\sin\theta(t_i)[X_j(t_0) + \frac{d_0}{Z_{0j}-l} - \frac{x_c(t_i)}{Z_{0j}-l}] + \cos\theta(t_i)[1 + \frac{l}{Z_{0j}-l} - \frac{v}{Z_{0j}-l}t_i] - \frac{l}{Z_{0j}-l}} + n_{X_j}(t_i)$$

$$Y_j(t_i) = f\frac{Y_j(t_0)}{\sin\theta(t_i)[X_j(t_0) + \frac{d_0}{Z_{0j}-l} - \frac{x_c(t_i)}{Z_{0j}-l}] + \cos\theta(t_i)[1 + \frac{l}{Z_{0j}-l} - \frac{v}{Z_{0j}-l}t_i] - \frac{l}{Z_{0j}-l}} + n_{Y_j}(t_i)$$

where $(X_j(t_0), Y_j(t_0))$ are the image plane coordinates of the j^{th} feature point at the beginning and can be found as follows:

$$X_j(t_0) = \frac{X_{0j} - h - d_0}{Z_{0j} - l}$$

$$Y_j(t_0) = \frac{Y_{0j}}{Z_{0j} - l}$$

If $x_c(t) \ll Z_{0j} - l$, the image plane displacement due to the bouncing movement is almost zero and the information is likely to be overridden by errors in feature tracking. Similarly, the spatial resolution of the images should be high enough that the image plane displacements due to the bouncing movement can be seen in the sequence.

Accordingly, the image sequence is assumed to be acquired at a rate of 10Hz. Each image is of size 2.0×2.0 and has resolution 2000×2000. The first four landmarks listed in Table 2 are tracked over the sequence in the simulation. Note that in generating these landmarks, it is further assumed that the landmarks close to the camera are likely to appear in the lower part of the images at the beginning. For simplicity, the landmarks are carefully chosen so that they remain in the field of view at all times.

Table 2: The 3-D coordinates of landmarks in the inertial coordinate system I

Landmarks	3-D coordinates			Landmarks	3-D coordinates		
1	−13.75	−15.75	22.50	5	−29.50	−31.50	45.00
2	−14.80	−8.40	21.00	6	−31.60	−16.80	42.00
3	−15.25	11.50	23.00	7	−32.50	23.00	46.00
4	−10.90	17.20	21.50	8	−23.95	34.60	43.25

As mentioned above, the movements of the unsprung elements need to be known in order to

apply the IEKF. Since they are obtained from the integration of measured accelerations, errors are expected. Uniformly distributed errors with variances proportional to the true values are therefore added to model uncertainties. For comparison, the resulting errors in the movements of the sprung element obtained from direct integration of (21) are shown in Figure 4.

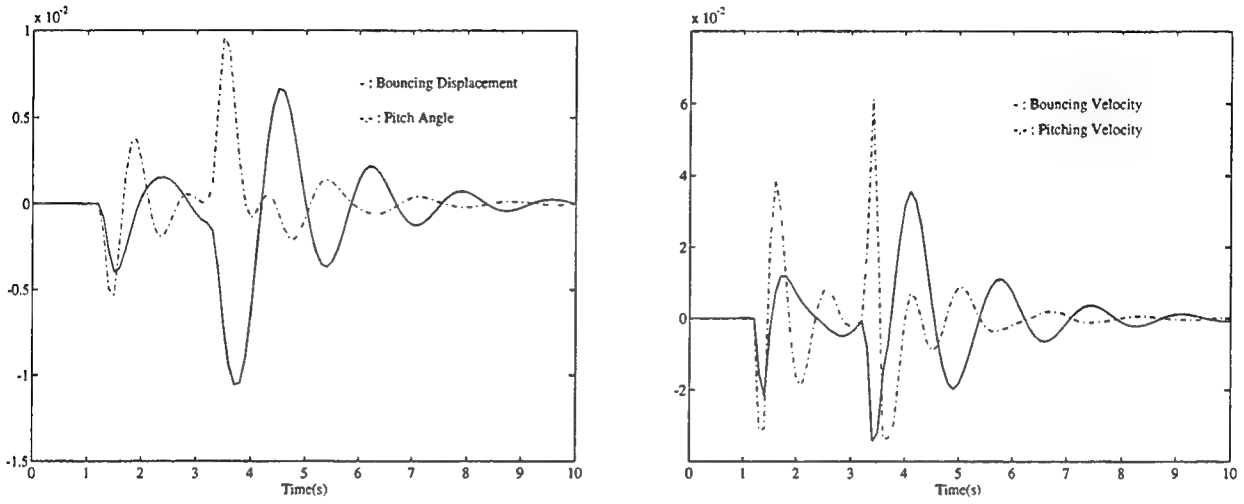

(a) (b)

Figure 4: The errors in the sprung element's movement obtained from direct integration (deterministic excitation): (a) The bouncing displacement and the pitch angle; (b) the bouncing velocity and the pitch velocity.

After the measurements and control inputs are obtained, assuming the vehicle is in the equilibrium state and moves forward at a speed of $1.0\ \mathrm{m} \cdot \mathrm{s}^{-1}$ initially, the bias and Root-Mean-Squared Errors (RMSE) obtained from twenty Monte Carlo runs are shown in Figures 5 and 6. Since the estimate of the forward speed is quite accurate, the corresponding result is not shown here.

To compare our results with other kinematic-model-based algorithms, a kinematic model which assumes that the camera moves with constant translation and rotation is adopted. The plant equation for the kinematic model is therefore

$$\dot{\underline{x}} = \tilde{A}\underline{x} + \underline{w} \tag{31}$$

where $\underline{x}$ is the state vector defined in (20), and $\tilde{A}$ is the sparse square matrix

$$\tilde{A} \equiv \{\tilde{A}_{12} = \tilde{A}_{34} = 1; \quad \text{all other elements } \tilde{A}_{ij} = 0\} \tag{32}$$

$\underline{w}$ is the plant noise.

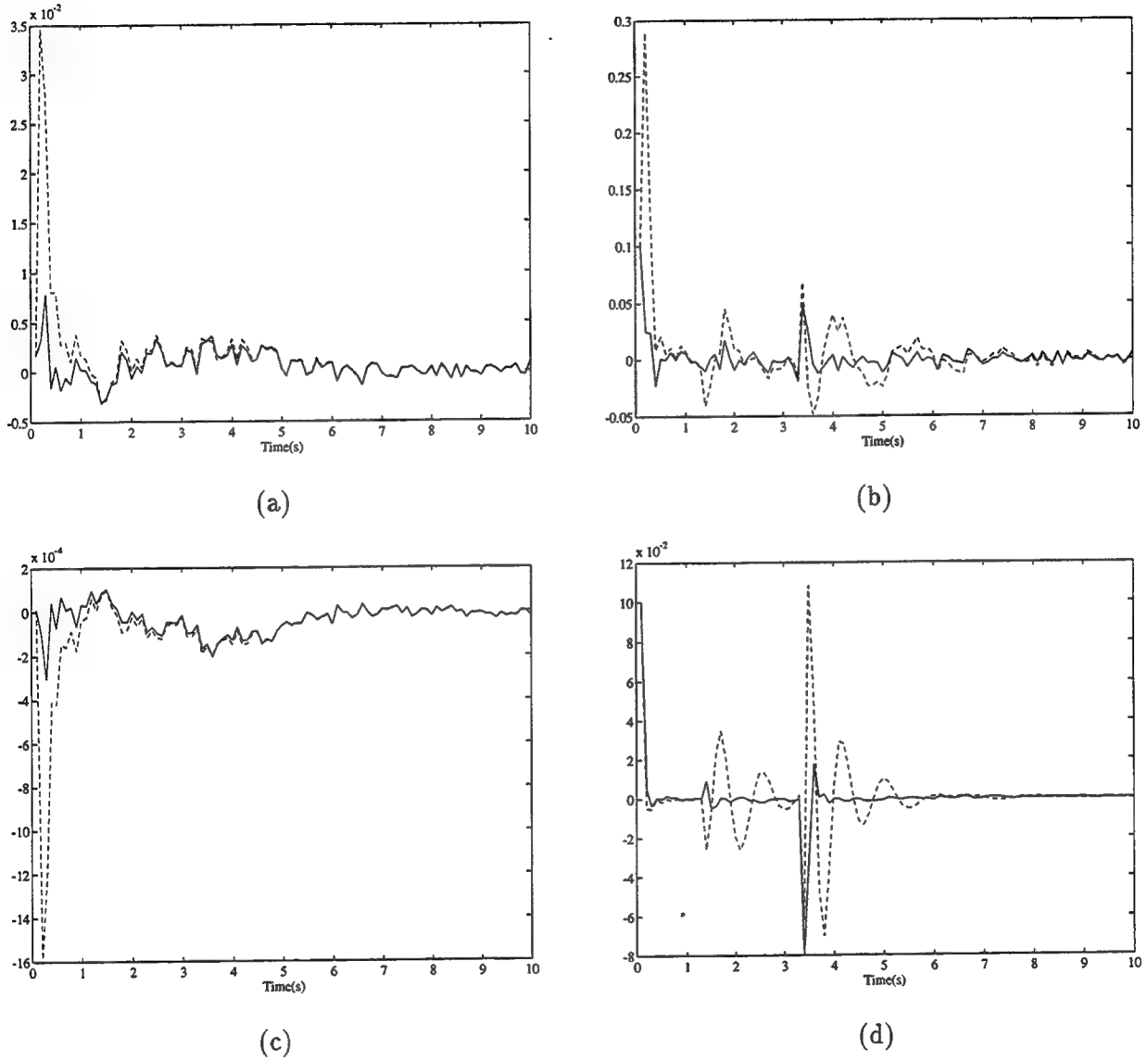

Figure 5: Bias in the estimates of the sprung element's movement under deterministic excitation for the kinetic (solid line) and kinematic (dashed line) models: (a) The bouncing displacement; (b) the bouncing velocity; (c) the pitch angle; (d) the pitch velocity.

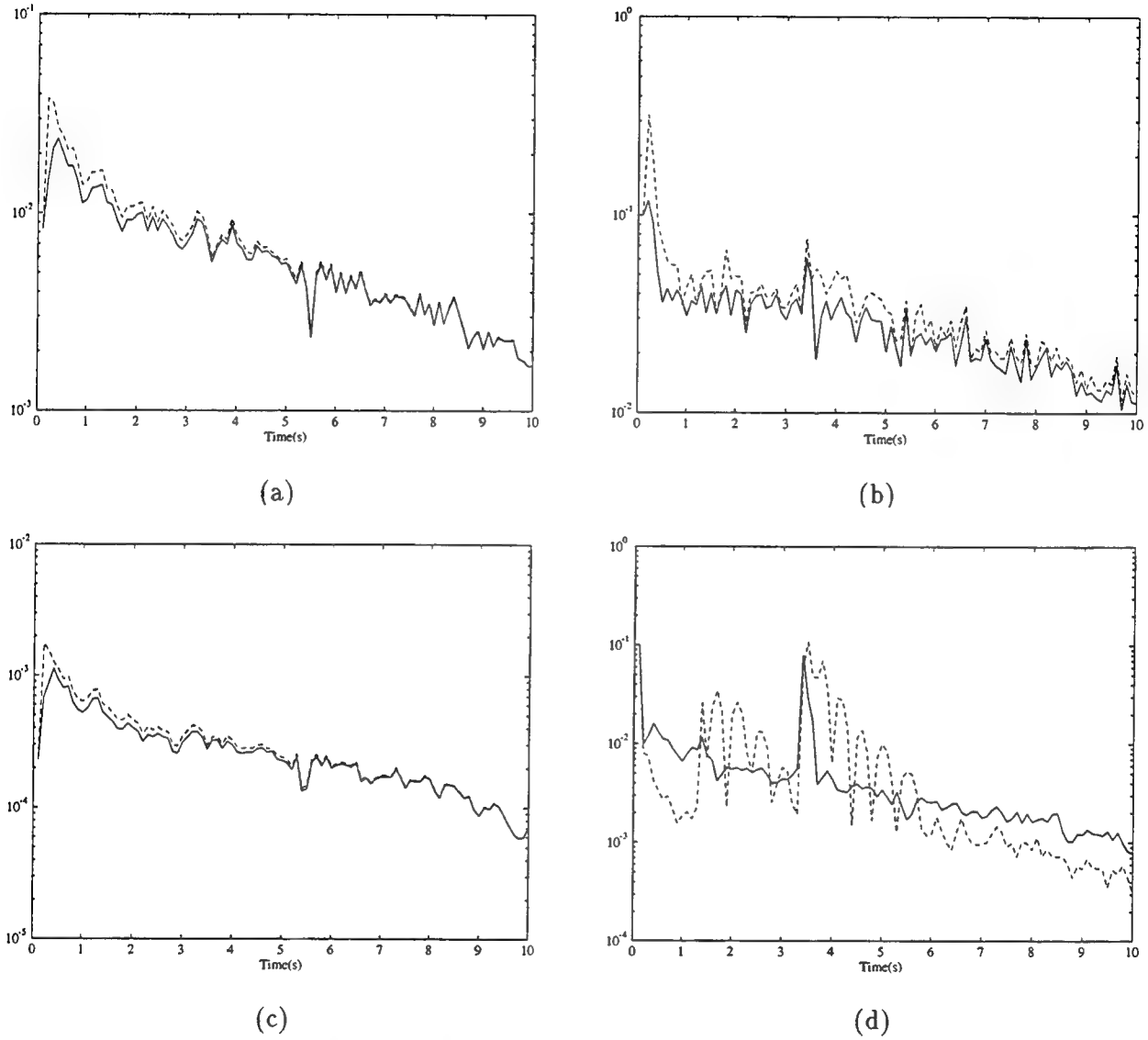

Figure 6: RMSE in the estimates of the sprung element's movement under deterministic excitation for the kinetic (solid line) and kinematic (dashed line) models: (a) The bouncing displacement; (b) the bouncing velocity; (c) the pitch angle; (d) the pitch velocity.

As seen from Figures 5 and 6, for $x_c(t)$ and $\theta(t)$, both models provide good yet similar estimates. This is due to the direct relationships between corresponding states and measurements. As for the other two states, $\dot{x}_c(t)$ and $\dot{\theta}(t)$, the kinetic model responds to the excitation faster than the kinematic model because of better modeling. In addition, it is observed that the estimates of $\theta(t)$ and $\dot{\theta}(t)$ are more accurate than the estimates of $x_c(t)$ and $\dot{x}_c(t)$ since the measurements provide different information as mentioned above.

Although the kinematic model provides estimates comparable to the kinetic model after the transient, there are irregularities continuously acting on the tires in the real world. We study the responses of both models under continuous irregularities in the next section.

4.2 Stochastic Excitation

For simplicity, the irregularity is modeled by a first order Markov process with coefficient depending on surface roughness and the vehicle's forward speed. Specifically, the excitation input to the front tire is modeled as

$$\dot{x}_{01}(t) = -a\,v\,x_{01}(t) + n(t) \tag{33}$$

where $n(t)$ is zero mean, white Gaussian noise with variance equal to $2\sigma^2 av$. The values of the coefficients, a and σ, vary with the roughness of surface. v is the vehicle's forward speed. In particular, $\sigma = 0.012$ m, $a = 0.40\ \mathrm{m}^{-1}$ and $v = 13.45\ \mathrm{m} \cdot \mathrm{s}^{-1}$ were chosen in our work [8]. Figure 7 shows a sample function of the random process. Then, according to (30), the excitation of the rear tire is also specified. The resulting movement of the sprung element is shown in Figure 8.

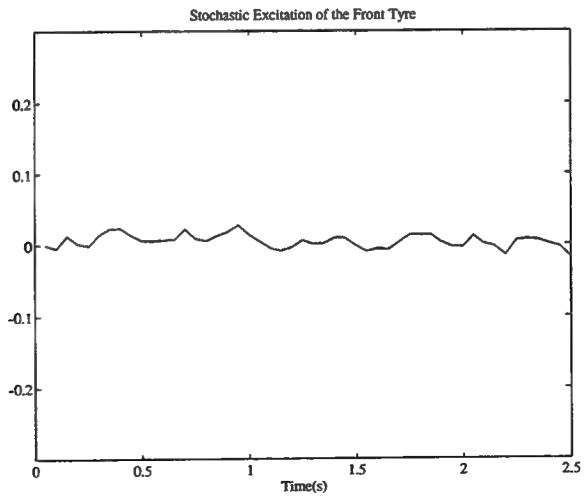

Figure 7: The stochastic excitation to the front tire.

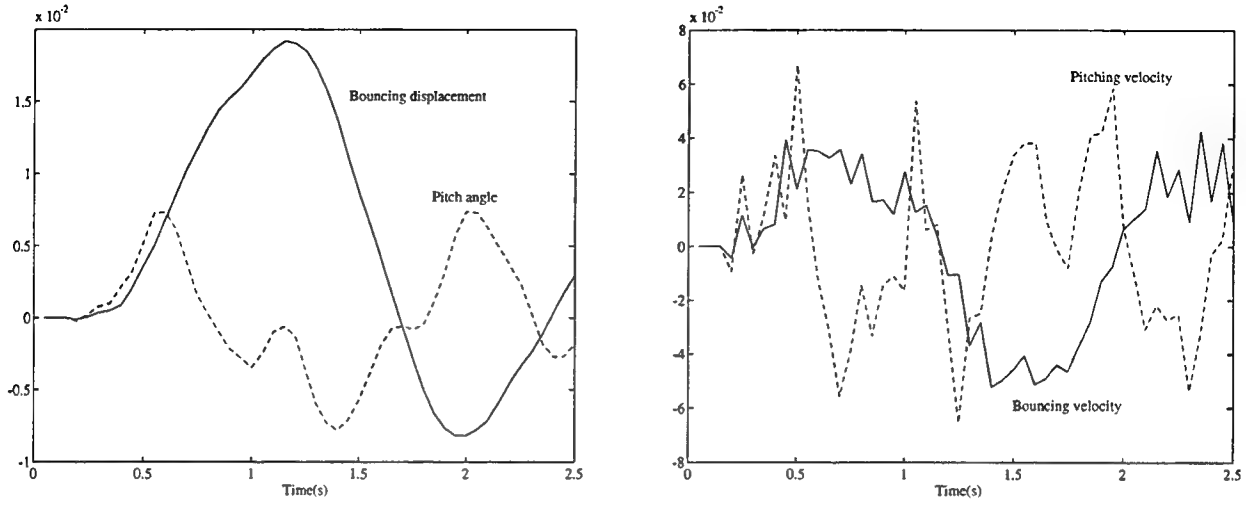

(a) (b)

Figure 8: The movement of the sprung element under stochastic excitation: (a) The bouncing displacement and the pitch angle; (b) the bouncing velocity and the pitch velocity.

Since the speed of the vehicle is higher, a higher image acquisition rate is assumed in this case. Accordingly, the last four landmarks listed in Table 2 are tracked and an image sequence is acquired at the rate of 20Hz in which each image has the same size and resolution as before. The choice of the last four landmarks is such that they remain in the field of view for more than three seconds. In addition, because the four landmarks are almost out of the field of view in three seconds, only fifty frames are considered.

As in the previous case, the movements of the unsprung elements are assumed to be noisy. Moreover, in estimating the motion of the sprung element, unlike the previous case, the vehicle is not in the equilibrium state when the processing begins. Instead, we assume the initially its center of gravity is 0.01 m higher than the equilibrium point, the bouncing velocity is equal to 0.1 $\mathrm{m} \cdot \mathrm{s}^{-1}$, the pitch angle is 0.01 rad, the pitch velocity is 0.1 $\mathrm{rad} \cdot \mathrm{s}^{-1}$, and the forward speed is 10.0 $\mathrm{m} \cdot \mathrm{s}^{-1}$. Then, with the initial conditions different from the exact starting states, the effects of imperfect knowledge are shown in Figure 9; the estimated results of both kinetic and kinematic-model based algorithms from twenty Monte Carlo runs are displayed in Figures 10 and 11.

As seen from the figures, the IEKF reaches a steady state quite quickly and improves its performance over direct integration by incorporating visual information. Furthermore, the kinetic model outperforms the kinematic model because of its better response to continuous irregularities.

Now that the performance of the filter with exact knowledge of a set of internal parameters has

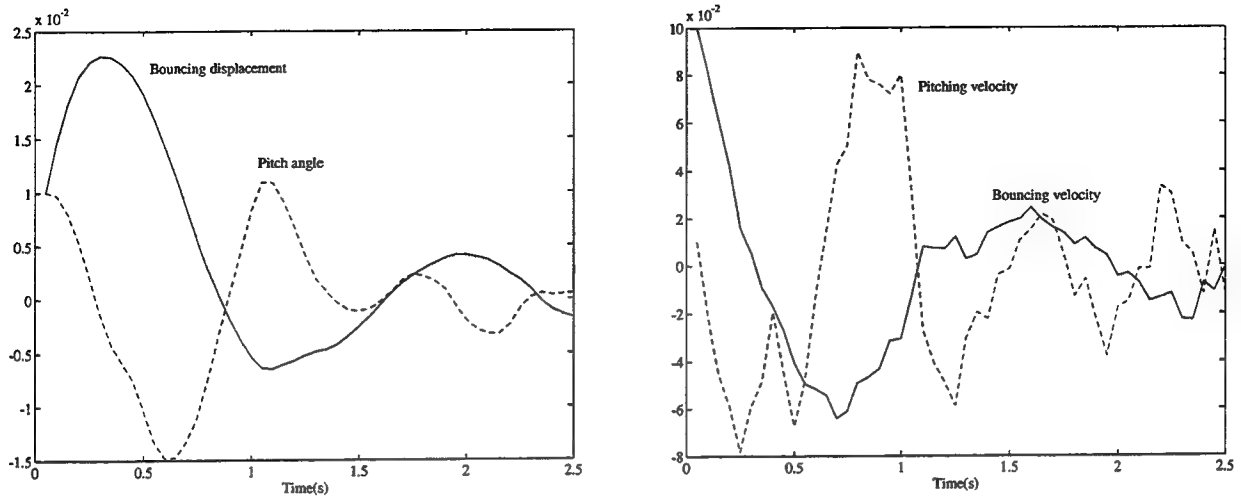

(a) (b)

Figure 9: The errors in the sprung element's movement estimated from direct integration (stochastic excitation): (a) Bouncing displacement and pitch angle; (b) bouncing velocity and pitch velocity.

been studied, the robustness issue needs to be addressed. In the next section we investigate the sensitivity of the filter to mismatches of various parameters.

5 Sensitivity Analysis

The proposed algorithm exploits knowledge not used by other kinematic-model-based algorithms to yield enhanced performance. However, to estimate the bouncing and pitching movements, a set of vehicle parameters needs to be known. In addition to the problem of measuring them precisely, some parameters are likely to vary during the operation of the vehicle, e.g. spring stiffness. It is therefore necessary to address the robustness of the filter.

In our formulation, since the wheel movements $\underline{x}_w(t)$ are approximately known, the effect of tire stiffness mismatch is not considered. The remaining parameters which affect the behavior of the model, i.e. the A and B matrices defined in (23), (24), are characteristic constants of the springs and dampers which consist of the suspension system, the vehicle mass M_B and moment of inertia I_{yy}, and the position of the center of gravity W_A. Note that because the sum of W_A and W_B is fixed, it is sufficient to study the effect of W_A only. In the following we present both analytic and numerical analysis results subject to the excitation input shown in Figure 7.

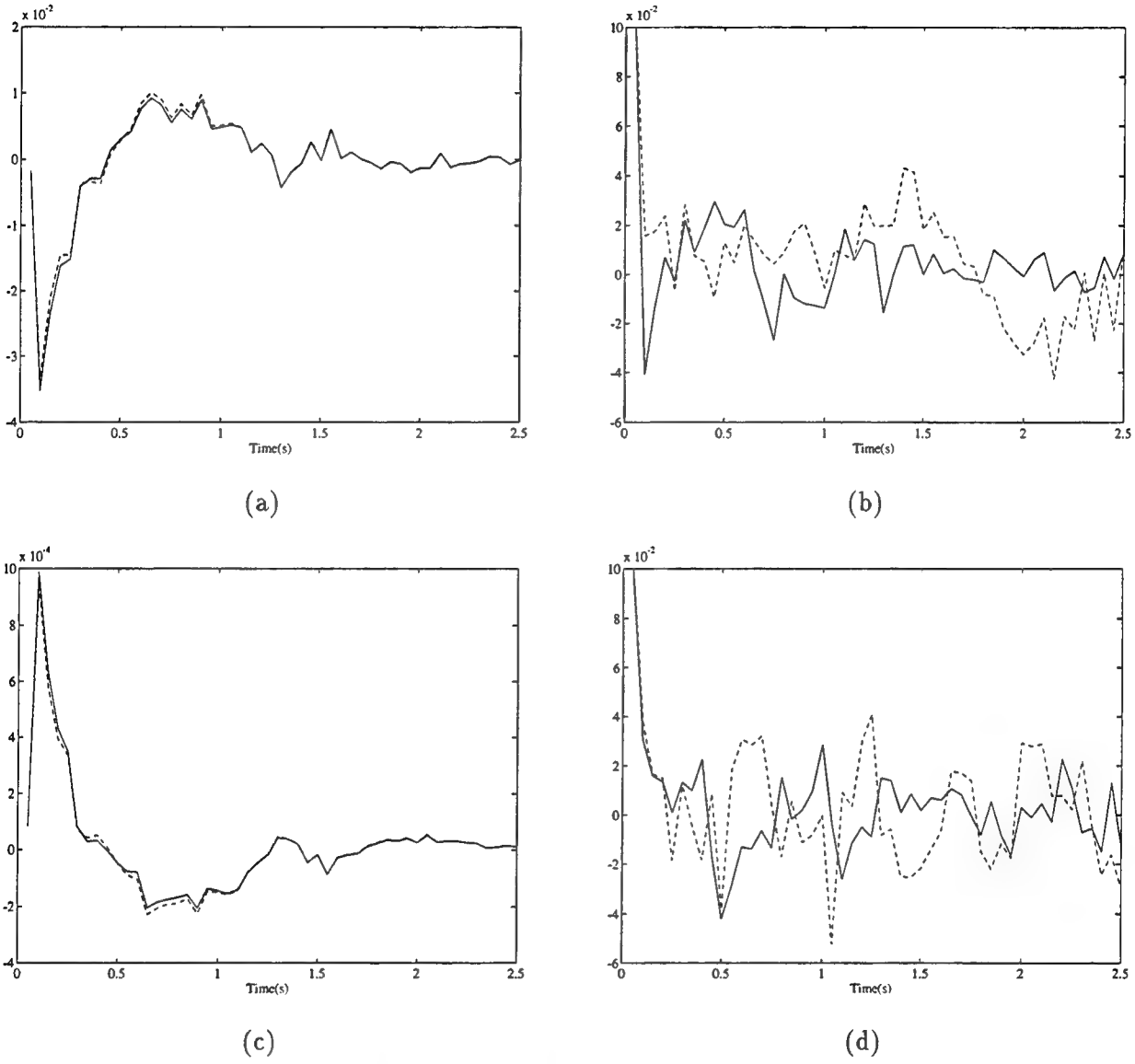

Figure 10: Bias in the estimates of the sprung element's movement under stochastic extitation for the kinetic (solid line) and kinematic (dashed line) models: (a) The bouncing displacement; (b) the bouncing velocity; (c) the pitch angle; (d) the pitch velocity.

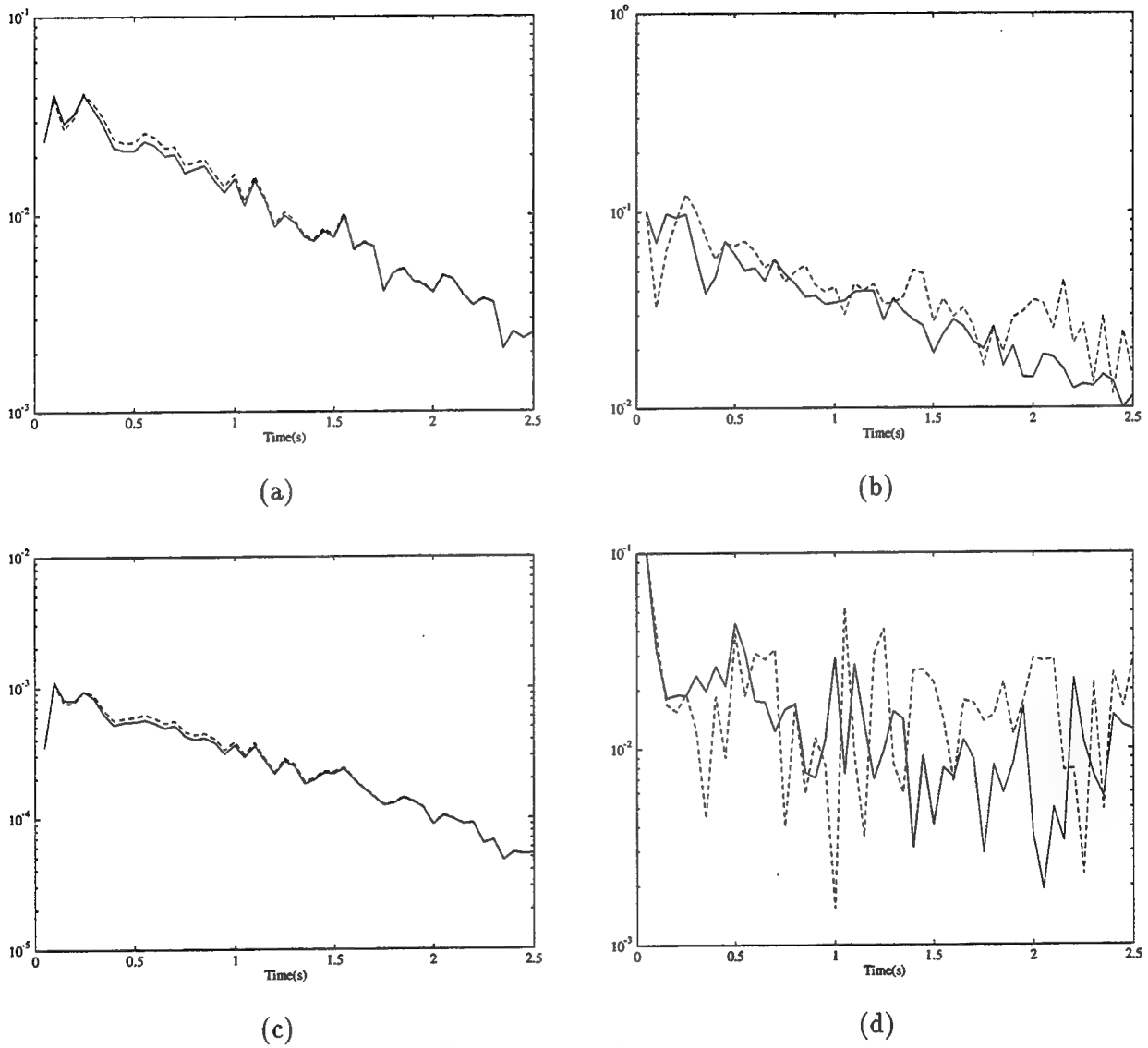

Figure 11: RMSE in the estimates of the sprung element's movement under stochastic excitation for the kinetic (solid line) and kinematic (dashed line) models: (a) The bouncing displacement; (b) the bouncing velocity; (c) the pitch angle; (d) the pitch velocity.

5.1 Analytic Sensitivity Analysis

The IEKF estimates the unstabilized components by combining the information in the dynamic model and visual data. As shown in the comparison of the kinetic and kinematic models, since not all of the states are directly related to the image plane movements of landmarks, it is important that the dynamic model provide a good description of these states. The sensitivity of the kinetic model to various parameters is therefore investigated.

For convenience, define the parameter vector $\underline{\lambda}$ as

$$\underline{\lambda} \equiv [K_f, K_r, C_f, C_r, W_A, M_B, I_{yy}]^T \tag{34}$$

and denote its nominal values by $\underline{\lambda}_0$. Then assuming the plant noise in (21) is zero, the dynamic model is described by

$$\dot{\underline{x}}(t,\underline{\lambda}) = A(\underline{\lambda})\underline{x}(t,\underline{\lambda}) + B(\underline{\lambda})\underline{x}_w(t) \tag{35}$$

$$\equiv f[\underline{\lambda}, \underline{x}(t,\underline{\lambda}), \underline{x}_w(t)] \tag{36}$$

The effect of parameter mismatches on $\underline{x}(t,\underline{\lambda})$ is studied using perturbation theory [6]. We focus on estimating the first order effect of parameter perturbations, say the sensitivity function. If we assume that $f[\underline{\lambda}, \underline{x}(t,\underline{\lambda}), \underline{x}_w(t)]$ is continuously differentiable with respect to $\underline{x}$ and $\underline{\lambda}$ and define the sensitivity function $S(t)$ as

$$S(t) \equiv \left.\frac{\partial \underline{x}(t,\underline{\lambda})}{\partial \underline{\lambda}}\right|_{\underline{\lambda}=\underline{\lambda}_0} \tag{37}$$

it can be shown [6] that when $||\underline{\lambda} - \underline{\lambda}_0||$ is sufficiently small, $S(t)$ satisfies the following differential equation:

$$\dot{S}(t) = F(\underline{\lambda}_0)S(t) + G(\underline{\lambda}_0, \underline{x}_w), \quad S(t_0) = 0 \tag{38}$$

where

$$F(\underline{\lambda}_0) = \left.\frac{\partial f}{\partial \underline{x}}\right|_{\underline{x}=\underline{x}(t,\underline{\lambda}_0)} \tag{39}$$

$$G(\underline{\lambda}_0, \underline{x}_w) = \left.\frac{\partial f}{\partial \underline{\lambda}}\right|_{\underline{x}=\underline{x}(t,\underline{\lambda}_0)} \tag{40}$$

and $\underline{x}(t,\underline{\lambda}_0)$ is the solution of (35) with the nominal values of the parameter vector.

Noting that $\underline{x}_w(t)$ is available, $S(t)$ can be easily obtained through numerical integration. Figure 12 shows the resulting $S(t)$. It has been observed that all the elements of $\underline{x}(t,\underline{\lambda}_0)$ are much more sensitive to W_A than the other parameters. In order to see the effects of mismatches in the

other parameters, the sensitivities of $\underline{x}(t, \underline{\lambda})$ with respect to W_A are shown in (a) and (b) separately. Figure 12 (c) to (f) show the sensitivities of each state to the other parameters. Since most of them are very small, we only show the effects of the three most sensitive parameters.

As seen from Figure 12, in addition to the high sensitivity to W_A, the bouncing movements are more sensitive to mismatches in M_B; the pitching behavior is more sensitive to mismatches in I_{yy}. Moreover, C_r has moderate effects on all the states, and the model seems to be less sensitive to spring stiffness mismatches.

Under the assumption that mismatches in the parameters are sufficiently small, the sensitivity function gives us a qualitative idea of how sensitive the model is to parameter mismatches. However, depending on the nominal values, mismatches can be moderate for some parameters, and the filter incorporates additional visual information to improve the estimates of both unstabilized components. The sensitivity of the filter to parameter mismatches is therefore studied quantitatively in the next section.

5.2 Monte-Carlo Simulations

Because of the effect of plant and measurement noise as well as imperfect knowledge of the unsprung elements' movements, sensitivity to parameter mismatches is studied through Monte Carlo methods. We focus here on the analysis for the stochastic excitation case. Therefore, using the parameters listed in Table 1 as nominal values, the ground truth for the states and measurement trajectories is generated as in Section 4.2. Then, by varying each parameter separately within a reasonable range, the performance of the filter is investigated.

In the following study, we first classify the parameters into three categories: suspension parameters, inertial parameters, and basic dimensions. Then, assuming the initial conditions of the IEKF are the same as those in the study of stochastic excitation, we present the effects of parameter mismatches in each category. For simplicity, since the bias in the estimates is small after the filter reaches the steady state, the average RMSE over the last 25 frames, i.e. $t \in [0.125, 0.25]$, is computed for comparison. With the nominal values listed in Table 1, the average RMS error in the estimate of $x_c(t)$ is 0.005911, in $\dot{x}_c(t)$ it is 0.021331, in $\theta(t)$ it is 0.000157, in $\dot{\theta}(t)$ it is 0.006673, and in v it is 0.002994.

(1) Suspension Parameters: The suspension parameters consist of K_f, K_r, C_f and C_r. For each component, two values corresponding to $\pm 50\%$ mismatches of the nominal value are consid-

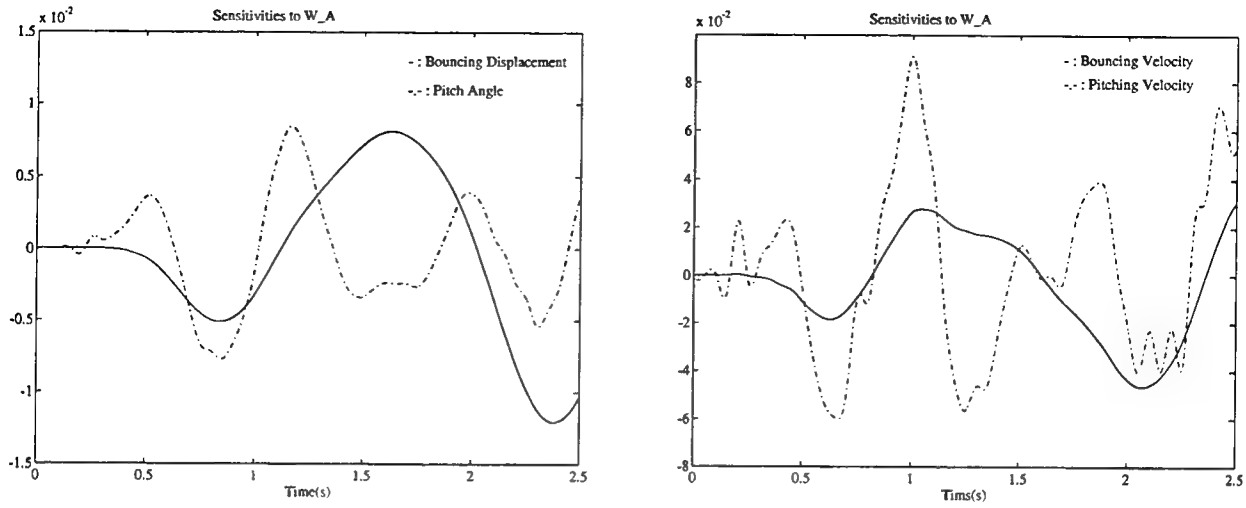

(a)

(b)

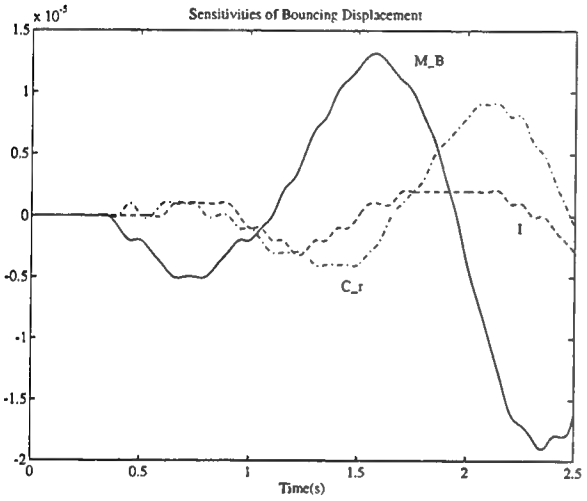

(c)

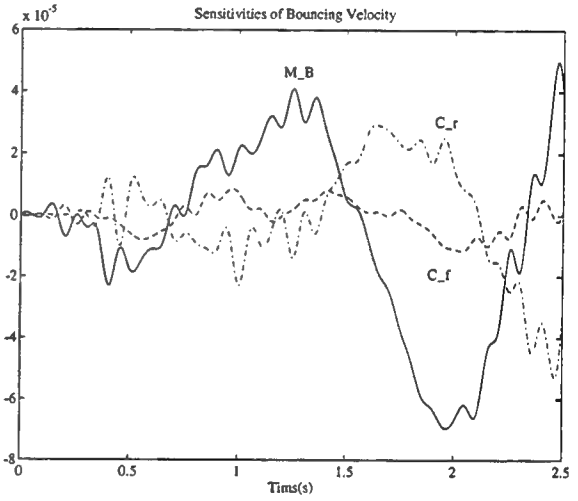

(d)

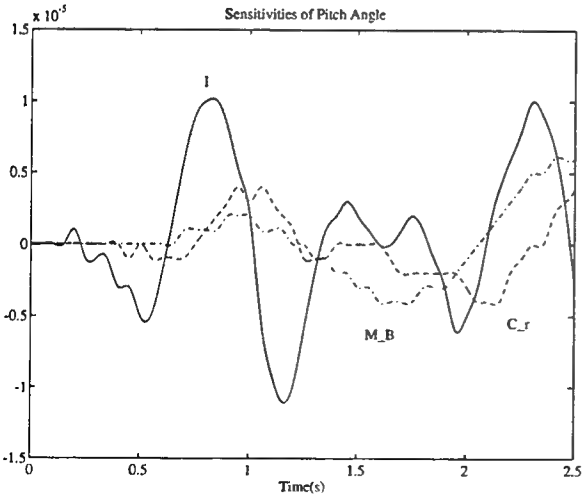

(e)

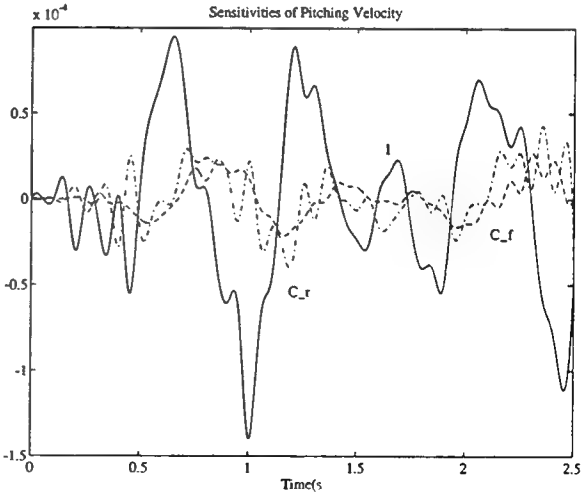

(f)

Figure 12: Sensitivity functions under random excitation.

ered. The resulting effects are shown in Table 3. Similar to the results shown in Section 4.2, $x_c(t)$ and $\theta(t)$ are insensitive to suspension parameter mismatches. As for $\dot{x}_c(t)$ and $\dot{\theta}(t)$, although the parameter mismatch is up to 50%, the performance of the filter degrades only a little.

Table 3: The effects of suspension parameters

Parameters			RMSE of $x_c(t)$	RMSE of $\dot{x}_c(t)$	RMSE of $\theta(t)$	RMSE of $\dot{\theta}(t)$	RMSE of v
K_f	9000.0	(−50%)	0.005747	0.019784	0.000138	0.007020	0.002500
	27000.0	(+50%)	0.005762	0.023697	0.000134	0.011747	0.002417
K_r	5000.0	(−50%)	0.005845	0.020547	0.000142	0.011751	0.002554
	15000.0	(+50%)	0.006084	0.023672	0.000164	0.007695	0.002916
C_f	500.0	(−50%)	0.005833	0.021439	0.000140	0.007078	0.002498
	1500.0	(+50%)	0.006040	0.021602	0.000167	0.006849	0.003027
C_r	500.0	(−50%)	0.005453	0.021577	0.000132	0.006453	0.002323
	1500.0	(+50%)	0.005800	0.020544	0.000149	0.008852	0.002772

(2) Inertial Parameters: We consider the mismatches of M_B and I_{yy}. Since these two parameters are directly related to the sprung element's movements, the performance of the filter is expected to be more sensitive to parameter mismatches. By varying each parameter separately by -50%, -25%, 25% and 50% of the corresponding nominal value, the average RMSEs resulting from the IEKF are shown in Table 4. As seen in Table 4, when M_B or I_{yy} is only half of the nominal value, the average error increases rapidly compared to the other cases. The model also seems to be more sensitive to smaller values of M_B and I_{yy}. Moreover, the mismatch of M_B only affects the estimates of $x_c(t)$ and $\dot{x}_c(t)$, but not those of $\theta(t)$ and $\dot{\theta}(t)$. The opposite is true for the effect of I_{yy}.

Table 4: The effects of inertial parameters

Parameters			RMSE of $x_c(t)$	RMSE of $\dot{x}_c(t)$	RMSE of $\theta(t)$	RMSE of $\dot{\theta}(t)$	RMSE of v
M_B	855.0	(−50%)	0.005453	0.031434	0.000140	0.006467	0.002593
	1282.5	(−25%)	0.005663	0.023491	0.000147	0.006285	0.002681
	2137.5	(+25%)	0.005749	0.021482	0.000142	0.006402	0.002453
	2565.0	(+50%)	0.006085	0.022240	0.000166	0.006645	0.003005
I_{yy}	515.6	(−50%)	0.005594	0.021763	0.000137	0.019551	0.002512
	773.4	(−25%)	0.006056	0.022475	0.000169	0.010187	0.003154
	1289.1	(+25%)	0.005902	0.021990	0.000151	0.006448	0.002811
	1546.9	(+50%)	0.005907	0.022386	0.000142	0.007306	0.002533

(3) Basic Dimensions: After the sensitivity to mismatches of the suspension and inertial parameters has been studied, W_A is the remaining parameter which affects the plant and input

matrices. The resulting performance of the filter when this parameter is mismatched by -50%, -25%, 25%, or 50% of the nominal value is shown in Table 5. As seen in Table 5, the filter is not very sensitive to mismatches in the parameter within 25%, but if the mismatch is too large, the error in the estimate of $\dot{\theta}$ starts to increase.

Table 5: The effects of basic dimensions

Parameters			RMSE of $x_c(t)$	RMSE of $\dot{x}_c(t)$	RMSE of $\theta(t)$	RMSE of $\dot{\theta}(t)$	RMSE of v
W_A	0.676	(-50%)	0.005627	0.020987	0.000143	0.012693	0.002629
	1.015	(-25%)	0.005708	0.022588	0.000151	0.007024	0.002813
	1.691	(+25%)	0.005607	0.022920	0.000131	0.009199	0.002191
	2.030	(+50%)	0.005624	0.025048	0.000149	0.012803	0.002917

Through our quantitative analysis, it is observed that the incorporation of visual information provides robust estimates of $x_c(t)$ and $\theta(t)$. And if the mismatches in various parameters are moderate, say less than 25% of the nominal values, the performance of the filter does not degrade much. Therefore, we claim that the filter is robust with respect to parameter mismatches.

6 Conclusions

A new kinetic-model-based algorithm has been presented for estimating some unstabilized components of vehicular motion. With the incorporation of existing kinematic-model-based motion estimation algorithms, a better description of the vehicular motion can be obtained. Consequently, many navigation-related tasks can be simplified. Although the 3-D landmarks are assumed to be known in this paper, structure from motion algorithms could be incorporated so that structure and motion could be estimated simultaneously. Because of improved modeling and the use of inertial sensors, better performance is possible.

In addition to its application to image understanding, the consideration of unstabilized components of vehicle motion provides information for improving the ride behavior of the vehicle. In order to compensate for the external disturbances, active suspension systems (which differ from passive systems in using the actuators to continuously generate forces acting on the wheels and vehicle body) have been suggested. Estimates of the unstabilized components can provide useful information in the design of active suspension systems.

References

[1] T.J. Broida and R. Chellappa, "Estimating the Kinematics and Structure of a Rigid Object from a Sequence of Monocular Images," *IEEE Trans. Patt. Anal. Mach. Intell.*, Vol. PAMI-13, pp. 497–513, June 1991.

[2] M. Demić, "Optimization of the Characteristics of the Elasto-damping Elements of a Passanger Car by Means of a Modified Nelder-Mead Method," *International Journal of Vehicle Design*, Vol. 10, pp. 136–152, 1989.

[3] E.A. Desloge, *Classical Mechanics*, vol. 2, New York:John Wiley & Sons, 1982.

[4] E.D. Dickmanns and B.D. Mysliwetz, "Recursive 3-D Road and Relative Ego-State Recognition," *IEEE Trans. Patt. Anal. Mach. Intell.*, Vol. PAMI-14, pp. 199–213, Feb. 1992.

[5] A. Hady and D.A. Crolla, "Theoretical Analysis of Active Suspension Performance Using a Four-wheel Vehicle Model," *Proc. Inst. Mech. Engrs*, Vol. 203, pp. 125–135, 1989.

[6] H.K. Khalil, *Nonlinear Systems*, New York: Macmillan Publishing Company, 1992.

[7] P.S. Maybeck, *Stochastic Models, Estimation, and Control*, vol. 2, New York: Academic Press, 1982.

[8] P. Michelberger, L. Palkovics, and J. Bokor, "Robust Design of Active Suspension System," *International Journal of Vehicle Design*, Vol. 14, pp. 145–165, 1993.

[9] I.H. Shames, *Engineering Mechanics, Volume II, Dynamics*, Englewood Cliffs, NJ: Prentice-Hall, Inc., 1980.

[10] C.N. Spentzas, "Optimization of Vehicle Ride Characteristics by Means of Box's Method," *International Journal of Vehicle Design*, Vol. 14, pp. 539–551, 1993.

[11] J. Weng, T.S. Huang, and N. Ahuja, "3-D Motion Estimation, Understanding, and Prediction from Noisy Image Sequences," *IEEE Trans. Patt. Anal. Mach. Intell.*, Vol. PAMI-9, pp. 370–389, May 1987.

[12] T.H. Wu and R. Chellappa, "3-D Recovery of Structural and Kinematic Parameters from a Long Sequence of Noisy Images," in *Proc. Image Understanding Workshop*, Washington, DC, pp. 641–651, April 1993. Accepted for publication, *International Journal of Computer Vision.*

[13] G.S. Young and R. Chellappa, "3-D Motion Estimation Using a Sequence of Noisy Stereo Images: Models, Estimation, and Uniqueness Results," *IEEE Trans. Patt. Anal. Mach. Intell.*, Vol. PAMI-12, pp. 735–759, Aug. 1990.

[14] Z. Zhang and O.D. Faugeras, "Three-Dimensional Motion Computation and Object Segmentation in a Long Sequence of Stereo Frames," *International Journal of Computer Vision*, Vol. 7, pp. 211–241, Aug. 1992.

REPORT DOCUMENTATION PAGE

Form Approved
OMB No. 0704-0188

1. AGENCY USE ONLY (Leave blank)	2. REPORT DATE	3. REPORT TYPE AND DATES COVERED
	September 1994	Technical Report

4. TITLE AND SUBTITLE

Estimation of Unstabilized Components in Vehicular Motion

5. FUNDING NUMBERS

DAAH04-93-G-0419

6. AUTHOR(S)

Yi-Sheng Yao and Rama Chellappa

7. PERFORMING ORGANIZATION NAME(S) AND ADDRESS(ES)

Computer Vision Laboratory
Center for Automation Research
University of Maryland
College Park, MD 20742-3275

8. PERFORMING ORGANIZATION REPORT NUMBER

CAR-TR-735
CS-TR-3349

9. SPONSORING / MONITORING AGENCY NAME(S) AND ADDRESS(ES)

U.S. Army Research Office
P.O. Box 12211
Research Triangle Park, NC 27709-2211

10. SPONSORING / MONITORING AGENCY REPORT NUMBER

ARO 32365.3-MA

11. SUPPLEMENTARY NOTES

The views, opinions and/or findings contained in this report are those of the author(s) and should not be construed as an official Department of the Army position, policy, or decision, unless so designated by other documentation.

12a. DISTRIBUTION / AVAILABILITY STATEMENT

Approved for public release; distribution unlimited.

12b. DISTRIBUTION CODE

13. ABSTRACT *(Maximum 200 words)*

This paper presents a kinetic-model based algorithm for estimating some unstabilized components in vehicular motion. In addition to smooth movement, there are unstabilized components such as bounce, pitch and roll in vehicular motion. To reliably accomplish other tasks like tracking and obstacle avoidance using visual inputs, it is essential to consider these disturbances. A two-wheel vehicle model available in the literature is used for this purpose. It takes into account the bouncing and pitching components. The dynamics of these unstabilized components are formulated using standard equations of motion. Assuming that depth information is known for some landmarks in the scene (e.g., obtained from a laser range finder) and additional information from inertial sensors such as accelerometers is available, a feature-based approach is proposed to estimate the unstabilized components. Simulation results for both deterministic and stochastic terrain profiles are presented. The robustness of the filter with respect to various parameter mismatches is also addressed.

14. SUBJECT TERMS

Dynamics, motion estimation, unstabilized components, vehicular motion

15. NUMBER OF PAGES

30

16. PRICE CODE

17. SECURITY CLASSIFICATION OF REPORT	18. SECURITY CLASSIFICATION OF THIS PAGE	19. SECURITY CLASSIFICATION OF ABSTRACT	20. LIMITATION OF ABSTRACT
UNCLASSIFIED	UNCLASSIFIED	UNCLASSIFIED	UL

GENERAL INSTRUCTIONS FOR COMPLETING SF 298

The Report Documentation Page (RDP) is used in announcing and cataloging reports. It is important that this information be consistent with the rest of the report, particularly the cover and title page. Instructions for filling in each block of the form follow. It is important to ***stay within the lines*** to meet ***optical scanning requirements***.

Block 1. Agency Use Only *(Leave blank)*.

Block 2. Report Date. Full publication date including day, month, and year, if available (e.g. 1 Jan 88). Must cite at least the year.

Block 3. Type of Report and Dates Covered. State whether report is interim, final, etc. If applicable, enter inclusive report dates (e.g. 10 Jun 87 - 30 Jun 88).

Block 4. Title and Subtitle. A title is taken from the part of the report that provides the most meaningful and complete information. When a report is prepared in more than one volume, repeat the primary title, add volume number, and include subtitle for the specific volume. On classified documents enter the title classification in parentheses.

Block 5. Funding Numbers. To include contract and grant numbers; may include program element number(s), project number(s), task number(s), and work unit number(s). Use the following labels:

C	- Contract	**PR**	- Project
G	- Grant	**TA**	- Task
PE	- Program Element	**WU**	- Work Unit Accession No.

Block 6. Author(s). Name(s) of person(s) responsible for writing the report, performing the research, or credited with the content of the report. If editor or compiler, this should follow the name(s).

Block 7. Performing Organization Name(s) and Address(es). Self-explanatory.

Block 8. Performing Organization Report Number. Enter the unique alphanumeric report number(s) assigned by the organization performing the report.

Block 9. Sponsoring/Monitoring Agency Name(s) and Address(es). Self-explanatory.

Block 10. Sponsoring/Monitoring Agency Report Number. *(If known)*

Block 11. Supplementary Notes. Enter information not included elsewhere such as: Prepared in cooperation with...; Trans. of...; To be published in.... When a report is revised, include a statement whether the new report supersedes or supplements the older report.

Block 12a. Distribution/Availability Statement. Denotes public availability or limitations. Cite any availability to the public. Enter additional limitations or special markings in all capitals (e.g. NOFORN, REL, ITAR).

- **DOD** - See DoDD 5230.24, "Distribution Statements on Technical Documents."
- **DOE** - See authorities.
- **NASA** - See Handbook NHB 2200.2.
- **NTIS** - Leave blank.

Block 12b. Distribution Code.

- **DOD** - Leave blank.
- **DOE** - Enter DOE distribution categories from the Standard Distribution for Unclassified Scientific and Technical Reports.
- **NASA** - Leave blank.
- **NTIS** - Leave blank.

Block 13. Abstract. Include a brief *(Maximum 200 words)* factual summary of the most significant information contained in the report.

Block 14. Subject Terms. Keywords or phrases identifying major subjects in the report.

Block 15. Number of Pages. Enter the total number of pages.

Block 16. Price Code. Enter appropriate price code *(NTIS only)*.

Blocks 17. - 19. Security Classifications. Self-explanatory. Enter U.S. Security Classification in accordance with U.S. Security Regulations (i.e., UNCLASSIFIED). If form contains classified information, stamp classification on the top and bottom of the page.

Block 20. Limitation of Abstract. This block must be completed to assign a limitation to the abstract. Enter either UL (unlimited) or SAR (same as report). An entry in this block is necessary if the abstract is to be limited. If blank, the abstract is assumed to be unlimited.